This paper describes objective technical results and analysis. Any subjective views or opinions that might be expressed in the paper do not necessarily represent the views of the U.S. Department of Energy or the United States Government.

SAND2021-0834J

Journal: Journal of The Electrochemical Society

Long-Term Effects of Humidity on Stainless Steel Pitting in Sea Salt Exposures

J. Srinivasan[1]*, T. D. Weirich[1], G. A. Marino[1], A. R. Annerino[1], J. M. Taylor[1], P. J. Noell[2], J. J. M. Griego[2], R. F. Schaller[2], C. R. Bryan[2], J. S. Locke[1], and E. J. Schindelholz[1]*

1: Fontana Corrosion Center, Department of Materials Science and Engineering, The Ohio State University, Columbus, OH 43210

2: Materials Science and Engineering, Sandia National Laboratories, Albuquerque, NM 87185

* Corresponding authors

Abstract

Ground 304 stainless steel (SS) samples were exposed to sea salt particles at 35 °C and two relative humidity (RH) levels for durations ranging from 1 week to 2 years. For all exposure times, pit number density and total pit volume at 40% RH were observed to be considerably greater than those at 76% RH. Statistical analysis of distributions of pit populations for both RH conditions showed that pit number density and total pit volume increased rapidly at first but slowed as exposure time increased. Cross-hatched features were observed in the 40% RH pits while ellipsoidal, faceted pits were observed at 76% RH. Optical profilometry indicated that most pits were not hemispherical. X-ray tomography provided evidence of undercutting and fissures. Piecewise curve fitting modeled the 40% RH data closely, predicting that corrosion damage would eventually plateau. However, a similar treatment of the 76% RH data suggested that corrosion damage would continuously increase, which implied that the piecewise power-law fit was limited in its ability to model atmospheric corrosion generally. Based on these observations, the operative mechanisms determining long-term corrosion behavior were hypothesized to be different depending on the RH of exposure.

Introduction

Studies on controlled atmospheric exposures of stainless steels to both individual and mixed salts have shown that relative humidity (RH) is a key driver of both the extent and morphology of pitting due to its effects on droplet size, electrolyte volume, and electrolyte

Sandia National Laboratories is a multimission laboratory managed and operated by National Technology & Engineering Solutions of Sandia, LLC, a wholly owned subsidiary of Honeywell International Inc., for the U.S. Department of Energy's National Nuclear Security Administration under contract DE-NA0003525.

chemistry.[1–5] However, these studies have focused primarily on pitting under microliter-sized droplets, which are often orders of magnitude larger than the volumes created by microscopic sea salt particles[6–9] present on surfaces in marine atmospheres. Additionally, the duration of these atmospheric exposures correspond to the early stages of pitting (hours or days), and do not characterize the data over longer time periods (up to years).[10–12]

A recent study by Weirich *et al.*[13] on 304 SS pitting under seawater droplets for one year in controlled atmospheric exposures showed that RH had a distinct influence on pit morphology. Pits grown at 40% RH displayed an irregular, cross-hatched morphology visually similar to the near-surface deformation caused by grinding. Fissures resembling microcracks were also present in association with pits. On the other hand, pits that developed at 76% RH displayed no such irregular morphology, instead forming crystallographically faceted ellipsoids with no associated microcrack-like fissures. The authors proposed that these differences were largely due to available cathodic resources provided by the humidity-dependent electrolyte conditions. The irregular morphology at low RH was attributed to the limited volume of $MgCl_2$-rich electrolyte which restricted cathode throwing power. Consequently, pit growth proceeded at conditions close to critical pit stability/repassivation. The hydrogen evolution reaction was hypothesized to be accelerated on the cathode surface due to the presence of high $MgCl_2$ content,[14] and at the corroding surface of the pit due to the increasing contribution of the local cathodic reaction near repassivation.[15] This possibility was reasoned to potentially lead to local hydrogen uptake and hydrogen-induced microcracking. At high RH, the larger volumes of NaCl-rich electrolyte allowed for greater cathodic throwing power, leading to higher polarization of the pit resulting in growth in more aggressive conditions, between critical pit stability and saturation. Overall, these results implied that RH played an influential role in determining susceptibility to pitting, microcracking, and possible eventual stress corrosion cracking (SCC).

Long-term pitting data are vital for corrosion-resistant design and management of various assets.[16,17] The design criterion of interest is a critical flaw size, such as depth of corrosion attack, that can be utilized in structural integrity analyses to assess susceptibility to mechanical failure due to SCC.[18] Statistically-based predictive models have typically generated estimates of this flaw size based on power-law relationships derived from regression of long-term empirical exposures to marine and industrial atmospheres.[10–12,19–23] However, the data for these models are usually based on outdoor exposures in uncontrolled conditions, which prevent a targeted study of how

specific environmental variables affect corrosion damage. Consequently, the predictive power of these models is highly local to the environment in which the data were generated, and as such their utility in predicting long-term pitting is still debated.[24–26]

Weirich *et al*.[13] sought to determine the effects of RH on the evolution of corrosion kinetics and damage morphology. The current work focused on whether the distinct differences in corrosion damage due to RH identified in that work[13] were consistently reproduced over a range of exposure duration encompassing both the initial stages of pitting as well as the mature evolution of pit growth. Ground 304 SS specimens loaded with sea salt microparticles were exposed to 40% and 76% RH from 1 week up to 2 years. Pits that developed on these surfaces were quantified and characterized using profilometry, electron microscopy, and X-ray microtomography. Data from the study were fit to power-law based predictive models to estimate long-term atmospheric corrosion behavior, with subsequent commentary on the mechanistic implications of these results.

Experimental

Material

The composition of the 304 stainless steel used in this study is shown in Table 1 and is identical to the material used in Weirich *et al*.[13] The parent material was a 4.76 mm-thick hot-rolled sheet (solution heat-treated at 1055 °C and water-cooled). The sheet surface was then ground to a standard #4 stainless steel finish with abrasive grinding belts of grit sizes 60 to 120 resulting in an average surface roughness (R_a) of 2.8 µm. Rectangular specimens of dimensions 25.4 mm × 50.8 mm laser-cut from this sheet were used in all experiments. Specimens underwent cleaning before exposure as follows: ultrasonication in acetone (3 minutes), ethanol rinse, ultrasonication in Liquinox® detergent (3 minutes), ultrasonication in deionized water (3 minutes), ethanol rinse, and finally drying with compressed nitrogen. These processing and preparation procedures were identical to those described in Weirich *et al*.[13]

Salt loading and environmental exposure

Specimens were printed with ASTM D1141 seawater at 80% RH and 21 °C using a LogoJet Pro H4 industrial inkjet printer. Uniform fields of picoliter droplet volumes (deposition density = 300 µg/cm^2) were obtained using this procedure. Two separate isohumidity chambers, one maintained at 40% RH and the other at 76% RH, were used to provide the exposure environment.

Both chambers were held at a temperature of 35 °C. In each chamber, a total of 21 printed specimens were placed. These specimens comprised of sets of three corresponding to seven different durations – 1 week, 2 weeks, 4 weeks, 26 weeks, 52 weeks, 78 weeks, and 104 weeks. Thus, a total of 42 specimens were exposed in the entire study. Each trio of specimens corresponding to each timepoint was removed at the end of that exposure duration from each chamber (*i.e.,* a total of six specimens were removed at every timepoint). Therefore, in each chamber, all specimens were exposed to the same RH (either 40% or 76%) and temperature conditions (35 °C) up until the point they were removed.

Post-exposure, specimens were cleaned and prepared for imaging and analysis as follows: scrubbing with a Nylon bristle brush in water, ultrasonication in 10 vol.% HNO_3 (30 to 120 minutes), rinsing in deionized water, and drying with compressed air. These methods were the same as described in Weirich *et al*.[13] Due to issues with printing uniformity, only one specimen each from both RH conditions at 104 weeks could be deemed usable for post-exposure analysis. The implications on data analysis and interpretation that arose from this limitation are considered in the Results and Discussion sections. For all the timepoints except 104 weeks, all three replicate specimens were usable post-exposure. Therefore, final analysis was performed on a total of 38 specimens.

Microscopy and optical profilometry

Pitting on the specimen surface was examined with a FEI Apreo FEG SEM operated at 20 kV and 1.6 nA. Pit density and morphology were characterized via optical profilometry (OP) with a GTK1 optical profilometer (Veeco Instruments Inc., USA) operated using green light with a 5× objective that provided a manufacturer-specified lateral resolution of 2 μm and a vertical resolution of <1 nm. The extent of pitting damage was quantified in terms of pit density (number of pits per unit area sampled) and total pit volume. The depth of the deepest pit identified in each specimen was also recorded. An automated find routine was implemented in the profilometer software which specified area and depth thresholds to identify pitting damage. The filtering thresholds were chosen as 10.4 μm and 200 μm^2. Pits shallower than this depth could not be unambiguously differentiated from surface features not associated with corrosion. The area threshold corresponded to the smallest resolvable pixel for the 5× objective. Manual filtering was additionally performed in order to remove any artifacts introduced during preparation which met the filtering threshold but

were incorrectly identified as pits by the software. In order to record the pit depth and diameter measurements, the zero-plane for the z-dimension was set to the mean of all z-values. Pit diameter was measured 10.4 μm below this zero-plane due to the threshold conditions adopted, and its value was determined by an average of the X and Y dimensions of the pit, as would fit within a rectangle. The pit depth was measured from the zero-plane to the bottom of the pit. This methodology was identical to the one described in Weirich *et al.*,[13] in which a graphic is provided to aid visualization.

For the samples exposed for 2, 4, 26, 78, and 104 weeks, the specimen surface that was imaged was divided into 24 equally spaced areas of 5 mm × 5 mm that together formed a rectangular sampling area that was a distance of 5 mm from the specimen edges. This method resulted in a sampling area of 6 cm^2. Data for the 52-week exposures were taken from previously published results[13] in which the specimen surface had been divided into three equally-spaced sampling areas of 12 mm × 12 mm with a perimeter clearance of 5 mm from the edges, providing a sampling area of 4.32 cm^2. The data for the 1-week exposures used in this study was also generated using this latter area sampling technique. OP was performed on one 52-week 76% RH exposure specimen using the 24-area sampling method and these data were compared with previously published results[13] using two-sample Kolmogorov-Smirnov (K-S) testing[27,28] to ensure that these two datasets were equivalent.

Tomography

An X-ray tomography (XCT) sample was machined from one of the specimens exposed for 52 weeks at 40% RH. The sample, which was ≈2.3 mm in diameter, was characterized using a lab-based Zeiss Xradia Versa 520 X-ray computed-tomography (XCT) system (Carl Zeiss XRM, USA). The XCT scan was performed using an accelerating voltage of 140 kV and a power of 10 kW using the Zeiss High Energy 2 (HE2) beam filter and a voxel size of 0.65 μm. For each dataset, a total of 3201 projections over 360° was taken with an exposure time of 13 s. Reference scans of the full beam without the sample taken at an interval of 350 projections were used for background subtraction and tomograph normalization. Radiographs from scans were automatically reconstructed by the Zeiss XM Reconstructor software using a standard filtered back-projection algorithm.

Reconstructed XCT datasets were processed using the Dragonfly Pro 3D software, version 3.1 (Object Research Systems (ORS) Inc., Canada). A non-local means filter was applied to the data using a kernel size of 5 and a smoothing of 1. Pits were manually segmented based on grayscale values and location. Segmented data were used to measure the volume and surface area of each pit. Errors in volume and surface area measurement were ±15% and ±10%, respectively. The largest diameter and deepest point of each pit were manually measured from the XCT images. OP using the same technique and filters mentioned previously was also carried out on one the XCT samples in order to compare the relative strengths of each technique toward corrosion feature resolution.

Results

Comparison of data obtained using different area sampling techniques

As described in the Experimental section, two-sample K-S testing was employed to ensure the equivalency of the 52-week data obtained using slightly different area sampling techniques. Results of this comparison are shown representatively for the 76% RH 52-week data in Figure 1. The data were observed to be not significantly different from one another at the $\alpha=0.05$ level. On this basis, data generated from the two area sampling techniques were deemed to be equivalent.

Pitting damage as a function of exposure time

Figure 2 presents the development of pitting damage for different exposure times at both RH values in terms of pit number density (number of pits per unit area) and total pit volume. Over the entire range of exposure time, pit number density at 40% RH was 3 to 6 times greater than that at 76% RH. Total pit volume was also higher at lower RH across all exposure times, with the data at 40% RH attaining nearly 10 times the corresponding value for each timepoint at 76% RH. For the 40% RH data, both pit number density and total pit volume appeared to approach a plateau after 26 weeks. For the 76% RH data, a similar approach to a plateau was less clear but the data at longer exposure times appeared to increase less steeply than at shorter times. This difference was also noted in the pit volume distributions plotted in Figure 3. For the 40% RH exposures, the pit volume distributions were seen to collapse into two groups on either side of the 26-week timepoint.

Such a clear separation was not seen for the 76% RH data. Two-sample K-S testing showed that for both RH conditions, pit volume distributions were not significantly different at the $\alpha=0.01$ level for exposure times greater than 26 weeks.

It should be noted that for all plots of profilometry data distributions in this paper, only one of three replicate samples corresponding to each timepoint is shown, with the exception of the 104-week data for which only one sample for each RH condition was usable (as mentioned previously in the Experimental Methods section). In addition to providing clarity in representation, this choice was justified based on two-sample K-S testing of the data, which indicated that the pit volume distribution for the exposures from each sample for every timepoint at a given RH was not significantly different at the $\alpha=0.01$ level. The replicate sample chosen for each timepoint was the one with the highest pit number density.

Figure 4 represents corrosion damage in terms of the deepest pit measured with respect to exposure time, which has been the parameter of choice to evaluate long-term exposures.[10,12,19,20] These data indicated that the depth of the deepest pit measured was consistently similar across different exposure times for both RH values considered, despite the noticeable difference in the corresponding corrosion pit volume (Figures 2 and 3).

Pit Morphology

As depicted in the series of SEM images in Figures 5 and 6, a distinct difference was noted in the pit morphology observed among the samples based on the RH condition of exposure. This difference was consistent at all exposure timepoints. As shown in Figure 5, pits that grew at 40% RH displayed an irregular, cross-hatched structure whereas pits that grew at 76% RH (Figure 6) presented a crystallographically faceted, ellipsoidal morphology. Further, micro-cracks were observed to be present only in the 40% RH exposures. These micro-cracks were typically detected at the periphery of pits and were observed in the data from all exposure durations, even in the ones as early as 1 week. These observations were consistent with the differences in pit morphology based on RH condition reported by Weirich *et al*.[13]

Supplementing the surface information from SEM, optical profilometry provided a quantitative means of characterizing pit morphology. Conventionally, pit diameter (or width) and pit depth have been used to describe pit shape.[4,5,19,29] These data can be combined in terms of a

single aspect ratio (*AR*) parameter – defined as *the ratio of the measured pit diameter to measured pit depth* – to provide a quantitative measurement of pit shape.

Pit diameter and depth values were extracted from the OP data (measured as described in the Experimental section) and the *AR* distributions for the two RH conditions across all exposure durations were calculated. The evolution of *AR* over time is depicted in Figure 7. These plots show that the majority of pits for both RH conditions were wider than they were deep ($AR > 1$). In general, the fraction of pits with $AR > 1$ was observed to decrease slightly as exposure time increased. From the plots in Figure 7, this fraction can be estimated as $(1 - f)$, where f is the cumulative probability value at which the distribution intersects the line indicating $AR = 1$. This fraction was observed to decrease from ≈90% initially to settle at ≈60-70% at long exposure times for both RH conditions.

It can also be observed from Figure 7 that for the 40% RH data, more than 70% of the pits at all exposure times have a lower *AR* than would be expected from a hemispherical pit ($AR = 2$). Correspondingly for the 76% RH exposures, more than 90% of pits at all exposure times had an $AR < 2$. Note however, that the value of $AR = 2$ is not unique to a hemispherical pit; a pit shaped like a regular cylinder or cone (radius = height) would also have the same *AR* value. Therefore, *AR* can be used to assess whether pits from large datasets are generally wider than they are deep but cannot differentiate unambiguously among pit shapes.

XCT provided subsurface pit information, particularly in terms of accessing features like fissures or undercutting[5,30], which might not be consistently captured by a line-of-sight technique like OP. Furthermore, XCT provides a nondestructive alternative to characterize such features compared to techniques like focused ion beam milling.[13,30] Images from individual XCT slices are presented in Figure 8, in which fissures emanating from the pit base and pit undercutting can be seen. Geometric data measured from the same sample using XCT and OP were compared and are shown in terms of distribution plots of pit depth, pit volume, and *AR* in Figure 9. It can be seen that OP has a greater lateral resolution as it detected a larger number of pits. Pit depths obtained from OP are observed to be greater than the XCT measurements (Figure 9 (a)). Note that one pit detected by XCT displayed a pit depth of <10.4 μm, which would have led to it being filtered from the OP data due to the threshold employed in the pit find routine. Pit volume measurements (Figure

9 (b)) were observed to be quite similar for the two techniques, particularly for larger pits, whereas there is some spread observed in the volume data as pits get smaller.

Discussion

The results of this study revealed that RH played an important role in determining corrosion damage and morphology for exposure durations from 1 week up to 2 years. In this section, the differences in quantitative corrosion damage observed in the two RH conditions are discussed in terms of pit number density, total pit volume, and deepest pit measured. Next, pit morphology differences due to RH are considered in the context of an electrochemical rationale established in the authors' previous work.[13] Thirdly, the utility of *AR* to quantitatively describe pit shape development with time is evaluated. Finally, the differences in observations of long-term corrosion damage between the two RH conditions are addressed in further detail. Toward this end, the efficacy of power-law-based models as predictive tools for atmospheric corrosion is assessed. A brief note on the statistical methods employed and the prospects and limitations of the experimental dataset generated by this study concludes this section.

Quantitative corrosion damage across exposure time

On average, the pit number density, total pit volume, and the deepest pit measured increase quickly for short durations before settling to a slower rate for the longer-term exposures, for both RH conditions, as shown in Figures 2 and 4. As exposure duration increased, the data up to and including 78 weeks for both RH conditions appeared to approach a plateau. The mean values of the pit number density and the deepest pit measured (Figures 2 (a) and 4) are slightly lower at 78 weeks than at 52 weeks, but the absence of replicates at the 104-week datapoint means that whether a true downward trend is represented by these data cannot be determined conclusively. Pit number density is governed by pit initiation, and the stochastic nature[31] of this phenomenon may lead to varying numbers of pits generated on independent samples at different exposure times. In Figure 4, The slightly lower mean value of the deepest pit measured at 78 weeks in comparison to the value at 52 weeks may have resulted due to the line-of-sight limitation of the OP technique failing to detect very deep pits at longer exposure times. Note however, that the mean total pit volume (Figure 2 (b)) at 78 weeks is slightly higher than that at 52 weeks for both RH conditions, while still within the limits of error to justify the rationale that they connote the approach to a plateau.

Therefore, the argument that corrosion damage approaches a limiting value with increasing exposure time is still valid.

Figure 4 also shows that all each timepoint, there is virtually no difference between the values of the deepest pit depth measured for either RH condition, which stands in sharp contrast to the fact that the total pit volume at 40% RH is consistently an order of magnitude is greater than that at 76% RH. Furthermore, the distinct difference noted between the morphology produced in the two humidity conditions is not captured by the deepest measured pit depth.

Pit morphology differences due to RH are consistent across time

In prior work,[13] distinct differences in morphology were observed between the pits that resulted from 40% RH and 76% RH exposed for 1 year. Exposure to 40% RH resulted in pits with an irregular, cross-hatched morphology while crystallographically faceted, ellipsoidal pits developed at 76% RH. As indicated by the SEM images in Figures 5 and 6, these differences were consistently reproduced in the current study at all exposure times The cross-hatched morphology of 40% RH implied that attack followed selective dissolution of a fixed active area due to growth at critical chemistry conditions[32]. Pit growth at 76% RH likely occurred at conditions between stability and saturation,[33] resulting in preferential dissolution along specific crystallographic planes which caused faceting. Despite the absence of an externally applied load, micro-cracks were observed to be present after 40% RH exposure even at times as short as 1 week. The fact that the distinct differences in morphology between RH conditions observed for a 1-year exposure in that study were consistently reproduced at all exposure times in the current investigation, it stands to reason that the working electrochemical hypothesis for the morphology differences presented in Weirich *et al*.,[13] (schematically depicted in Figure 10) would be applicable here as well. Weirich *et al*.[13] commented that low RH conditions may contribute to SCC initiation via hydrogen environment-assisted cracking (HEAC) due to a higher hydrogen availability at the corroding surface due to pit growth at conditions close to repassivation acting in concert with residual stresses and strain-induced martensite originating from surface deformation. The results from the current study suggest that a similar set of circumstances may be at play, thus indicating that low RH conditions may result in a higher susceptibility to SCC at all exposure times.

Pit shape deviates significantly from a smooth-surfaced hemisphere

Aspect ratio (*AR*) provides a quantitative basis to compare the pit morphology using pit depth and diameter. However, its utility to differentiate among pit shapes and to assess whether pits approximate a hemisphere is limited because several pit shapes may have the same *AR* value. Nonetheless, as a companion to qualitative evidence from SEM imaging or when only pit depth and diameter data are available, *AR* provides a useful quantitative tool to evaluate pit shape development.

As indicated by the *AR* data in Figure 7, the majority of all the pits detected were wider than they are deep, *i.e.* $AR > 1$. For longer-term exposures, the fraction of pits with $AR > 1$ appeared to converge to ≈60-70%. It was noted that *AR* decreased slightly as exposure time increased. This decrease may be due to the lower likelihood of equiaxial pit growth at long times. If equiaxial growth is to continue, the correspondingly increasing anodic demand has to be constantly matched by the cathodic supply. This condition is less likely to be met as growth progresses because the cathode is finite.[34,35] One possible manner in which pit growth could respond to this limiting cathode current would be to grow in more restricted geometry which requires a lower critical anodic stability parameter.[29] This restriction would then result in pits with a tendency to grow in depth rather than width as the exposure duration increased.

In Figure 9, which compared the measurements obtained from OP and the XCT techniques, the OP geometric data were, on average, greater than the corresponding XCT measurements. In particular, as observed in Figure 9 (a), the argument that XCT would resolve features more clearly than OP with respect to line-of-sight detection limitations could not be borne out. However, owing to the single sample studied and the low number of pits identified in the area mapped (8 for XCT, 14 for OP), the evidence in this study is not sufficient to conclusively rule out this potential advantage either. On a related note, it must be pointed out that the subsurface sources of pit depth measurement cannot be uniquely identified by OP. XCT scans, on the other hand, can permit mapping geometric data on to specific subsurface morphology like undercuts and fissures. It is therefore advantageous to use both techniques complementarily, as OP can provide better lateral resolution while XCT can identify and isolate critical subsurface features.

Long-term evolution of pitting damage

RH was observed to be a differentiating factor in long-term pitting development. Pit number density and total pit volume were both observed to increase much more slowly at long exposure times than at shorter durations. The 40% RH data appeared to approach a plateau at very long exposure times whereas this trend was not as clear with the 76% RH data. These results suggest that in both cases, pitting progress was curbed,[25,34] albeit to different degrees. This difference in the suppression of pit growth may arise due to changes in electrolyte coverage as corrosion proceeds and the consequent effects on pitting kinetics, as will be discussed in further detail in this section.

Power-law models based on the deepest pit measured have typically been used to provide long-term predictive damage estimates for atmospheric corrosion.[10,12,20] However, as was discussed previously in the context of Figure 4, the measured depth of the deepest pit did not provide information on the marked differences in pitting damage due to different RH conditions. Instead, total pit volume may be a more useful parameter in this regard, as it has been observed in this study to depend more sensitively upon the RH of exposure. Figure 11 shows plots with linear fits for the time-dependence of the measured depth of the deepest pit and the total pit volume data at each RH, as log-log plots. This representation is equivalent to a power-law fit. Figure 11 (a) reinforces the notion that the measurement of the depth of the deepest pit does not, on its own, accurately portray the RH-dependent differences in corrosion damage observed. Note also that employing the power-law fit for the time-evolution of total pit volume data in Figure 11 (b) does not indicate any trend toward slower growth at longer exposure times but forecasts instead that corrosion would indefinitely increase in a near-linear fashion.

Conventional power law models therefore have drawbacks as predictive tools for corrosion damage and structural integrity assessment under conditions similar to this study. For example, the conventional parameter used for comparison – deepest pit measurement – by itself does not discriminate among the extensive differences in pitting damage observed between the two RH levels in this study. Despite the deepest pits in either case having similar measured depths, the measured pit volume at 40% RH was considerably higher than that at 76% RH. Furthermore, with a view toward structural integrity, morphological features like the fissures and micro-cracks that develop in the 40% RH exposures may be especially susceptible toward SCC initiation as they are

likely to produce a high stress intensity factor.[13,36–38] Such nuances are not accounted for when the deepest measured pit depth alone is considered as a corrosion damage parameter.

Models based on a single power law to describe the entire range of exposure durations studied have not adequately predicted long-term corrosion behavior for passive oxide-forming alloys.[11,19,21,25,29] Schaller *et al*.[25] have however shown that a piecewise fitting method based on power law relationships could satisfactorily model a plateau in pit growth on aluminum due to stifling caused by brine dryout and/or precipitation. This approach included a second power law relationship to capture average corrosion rates approaching zero at long exposure times. A similar methodology applied to the data in this study resulted in the plots in Figure 12. In this analysis, two power-law expressions were used – one for the growth up to 26 weeks, and another to model the slower growth trending toward a plateau for longer exposure times. The parameters for the fitting equations are summarized in Table 2. The transition of 26 weeks was chosen based on the results in Figure 3 as it was the timepoint after which no significant difference at the α=0.01 level was observed following K-S testing of the pit volume distributions for both RH conditions.

Figure 12 (a) shows that piecewise curve fitting modeled the 40% RH data at all timepoints closely. As observed in Figure 12 (b), predictive extension of this model up to 10 years (500 weeks) indicated an approach to a plateau in corrosion damage. However, a similar treatment met with less success for the 76% RH data, as the fitting function predicted steadily increasing growth at very long exposure times. In particular, the availability of only one sample for the 104-week data for 76% RH condition appeared to skew the fit towards higher estimated damage.

These differences in predicted damage suggest that models based on power laws alone do not uniformly describe long-term corrosion behavior at different RH conditions. Note that power law models are used to predict corrosion damage based on the controlling process being oxygen diffusion through uniform corrosion product layers.[26] Such modeling has been shown to be largely appropriate for corrosion of copper[39] and carbon steels,[40] and has been extended to aluminum.[25,41] Modeling of long-term stainless steel pitting behavior, on the other hand, has been based on the galvanic separation of electrodes and has typically not considered any contribution to cathodic limitation from corrosion products.[34,35,42,43] However, in all such prior work on stainless steel, the electrolyte geometry has been assumed to be a continuous, uniform thin film. Weirich *et al*.[13] have discussed that for sea salt exposures on stainless steel, RH differences could contribute to changes

in electrolyte volume and the likelihood of secondary spreading,[44] both of which would affect electrolyte geometry. At 40% RH, the alkalinization of the Mg^{2+}-rich electrolyte due to the oxygen reduction reaction (ORR) could lead to the precipitation of insoluble magnesium hydroxide species. Similar precipitation would be less likely at 76% RH as the corresponding alkaline species in the Na^{+}-rich electrolyte would remain soluble.

This reasoning presents a possible explanation for the fact that the piecewise fitting closely modeled only the 40% RH data in the current study. Long-term atmospheric corrosion in the presence of insoluble salts precipitating due to brine dryout and changes in pH may physically provide the same conditions as a system with a large volume of corrosion products. This rationale can be developed analogous to the argument presented by Schaller *et al*.[25] for atmospheric corrosion of aluminum under NaCl droplets. In that paper, it was postulated that as corrosion proceeded, the interaction among aluminum ions from metal dissolution, alkalinization of electrolyte due to the ORR, and the presence of atmospheric CO_2 would result in the generation of an insoluble precipitate of dawsonite ($NaAlCO_3(OH)_2$). Such precipitation would then consume the electrolyte and thereby shut off cathodic current, limiting further pit growth. In this study, a similar mechanism may be at play for the 40% RH exposures, with the precipitation of insoluble alkaline magnesium species,[14] due to the secondary spreading phenomenon discussed previously. Using the same logic to argue the contrary for the 76% RH exposures, cathode shutoff due to precipitation would be less likely for the Na^{+}-rich electrolyte, because of the higher solubility of the resultant alkaline sodium species.[14]

The maximum pit size model[29,34] may provide some headway toward a preliminary mechanistic rationale for the long-term corrosion behavior of the 76% RH exposures observed in this study. This reasoning is justified by the fact that the electrolyte in high RH conditions tends closer toward a thin film geometry due to the high electrolyte volume and secondary spreading.[13] The finite cathodic current available under a thin film would therefore be distributed among multiple individual pits. Additionally, based on the pit morphology observed, the electrochemical conditions for pit growth at higher RH require a higher critical pit stability product and therefore a higher anodic current demand, as has been schematically illustrated in Figure 10. Consequently, the overall size to which pits can grow at 76% RH would be restricted. Based on the reasoning provided previously, the higher solubility of alkaline sodium species implies that brine

displacement by precipitation is less probable at 76% RH.[13,44–46] The onset and development of pit stifling in these circumstances would therefore be gradual compared to the more abrupt impact of cathode shutoff expected at 40% RH.

Limitations and prospects of the data analysis in current study

The various limitations of the experimental dataset and the associated analysis presented in this work have been discussed in prior sections and they are reviewed in summary here, in the context of identifying prospects for future study. Firstly, optical profilometry, by nature a line-of-sight technique, may not have captured extremely narrow fissures, thereby returning a shallower pit depth measurement. The efficacy of XCT in circumventing this issue was assessed in the current study; however, the results from these measurements were not conclusive due to the low lateral resolution associated with the present technique employed. Data from larger area XCT scans may help to overcome this limitation.

Secondly, the lack of replicate data for 104 weeks mandates particular caution in data interpretation at this timepoint, as the unavailability of additional samples prevented an extensive comparative discussion of the experimental scatter of pit number density, total pit volume, and deepest pit measured with respect to the immediately preceding exposure timepoints. This limitation is underscored in the piecewise power-law fits, particularly for 76% RH. One possible path to rectify this issue would be to observe whether replicate data from still longer experimental exposures (130 weeks, 156 weeks, 208 weeks) are modeled closely by the extrapolation from the fits in this study. Such longer-term data would also be useful, in addition to those generated in this study, as input for a generalized extreme value (GEV) model-based treatment.[47]

The primary purpose of this study was to provide the experimental evidence that RH influences corrosion damage and pit morphology consistently across a range of exposure duration. The results presented suggest that long-term atmospheric corrosion in stainless steel is likely governed by mechanistically distinct processes whose relative dominance is dependent on the RH of the exposure environment. The power-law model used in this study as a tool to provide some predictive insight into long-term corrosion development was intended to highlight the effects of these mechanistic differences. The statistical treatment of the data in this study was therefore not meant to serve as an alternative to extreme value distributions such as Weibull and Gumbel fits

that provide estimates for the limiting size of corrosion damage.[22,23,48] To incorporate these results into a larger discussion of predictive statistics for pitting, the individual datasets provided in the supplementary information could be used for the development of GEV-based and other targeted models for long-term atmospheric corrosion. An in-depth discussion of long-term predictive statistics would therefore be outside the immediate focus of this particular study.

Thirdly, although the authors recognize that the K-S test is not the most powerful technique to test similarity of distributions,[49,50] its utility as an quantitative basis for empirical data comparison lies in the fact that it specifically does not require knowledge of the underlying parent distributions of the data being compared. This aspect made it appropriate for use in the current study. Note that the K-S test was employed in this study primarily to provide an initial quantitative basis to evaluate whether RH plays a differentiating role in corrosion damage distribution trends at long exposure times and assess the underlying mechanistic causes of such differences.

Finally, the long-term trends for the 76% RH data in this study were qualitatively evaluated using the maximum pit size concept formulated by Kelly and coworkers.[34] A quantitative form of this argument requires further study, incorporating time-dependent changes in electrolyte geometry and chemistry[51] in the maximum pit size model framework. Sensitivity analysis of the cathodic current with respect to precipitation and brine dryout, similar to the work of Katona *et al.*[52] for chloride solutions, would help to identify RH ranges across which either mechanism may be dominant.

Conclusions

Overall, this work investigated the effects of RH on pitting damage development at various exposure times. Exposure at two RH conditions for up to 2 years provided the scope to observe variations in pit morphology, density, and pit volume. The key conclusions reached in this study are as follows:

- RH distinctly influenced pit number density, pit volume, and morphology at all exposure durations. Irregular, cross-hatched pits containing microcracks were observed in the 40% RH exposures. The 76% RH exposures produced crystallographically faceted ellipsoids. Pit number density and total pit volume were consistently observed to be higher at 40% RH than at 76% RH across all exposure times.

- Pit shape quantified in terms of aspect ratio (*AR*) indicated that virtually all the pits were not hemispherical but were generally wider than they were deep (*AR* > 1).
- Pit density and pit volume both appeared to approach plateaus at long exposure times. This trend in pit volume was more evident for the 40% RH data than for 76% RH. Piecewise curve fitting with power law expressions provided some preliminary predictive insights. A long-term plateau in total pit volume was predicted for 40% RH whereas total pit volume was predicted to continuously increase with exposure time for 76% RH. These results suggested that different mechanisms, based on the exposure RH, may determine long-term corrosion damage development. The presence of insoluble precipitates leading to cathode shutoff was qualitatively theorized to be responsible for long-term behavior at 40% RH. A more gradual stifling of pit growth at long times in response to cathode sharing among multiple pits may occur in the case of 76% RH.

Acknowledgments

This work was supported at The Ohio State University by Sandia National Laboratories, a multi-mission laboratory managed and operated by National Technology and Engineering Solutions of Sandia LLC, a wholly owned subsidiary of Honeywell International Inc. for the U.S. Department of Energy's National Nuclear Security Administration under contract DE-NA0003525. Additional support was provided by the Center for Performance and Design of Nuclear Waste Forms and Containers (WastePD), an Energy Frontier Research Center funded by the U.S. Department of Energy, Office of Science, Basic Energy Sciences under Award # DE-SC0016584, and by the Laboratory Directed Research and Development (LDRD) program at Sandia National Laboratories. This paper describes objective technical results and analysis. Any subjective views or opinions that might be expressed in the paper do not necessarily represent the views of the U.S. Department of Energy or the United States Government. The authors would like to thank Dr. Stephanie DeJong, Sandia National Laboratories, for discussions regarding the appropriateness of K-S testing as applied in this study. JS would like to thank Dr. Zachary D. Harris, University of Virginia, for helpful discussions and assistance with piecewise curve fitting.

Data Availability

All data used in this study are uploaded as Supplementary Information at the link in the web version of this article, and their use is permitted in future studies once properly attributed.

References

1. S. R. Street, N. Mi, A. J. M. C. Cook, H. B. Mohammed-Ali, L. Guo, T. Rayment, and A. J. Davenport, *Faraday Discuss.*, **180**, 251–265 (2015).

2. C. Padovani, O. E. Albores-Silva, and E. A. Charles, *Corrosion*, **71**, 292–304 (2015).

3. A. J. M. C. Cook, C. Padovani, and A. J. Davenport, *J. Electrochem. Soc.*, **164**, C148–C163 (2017).

4. L. Guo, S. R. Street, H. B. Mohammed-Ali, M. Ghahari, N. Mi, S. Glanvill, A. Du Plessis, C. Reinhard, T. Rayment, and A. J. Davenport, *Corrosion Science*, **150**, 110–120 (2019).

5. L. Guo, N. Mi, H. Mohammed-Ali, M. Ghahari, A. Du Plessis, A. Cook, S. Street, C. Reinhard, R. C. Atwood, T. Rayment, and A. J. Davenport, *J. Electrochem. Soc.*, **166**, C3010–C3014 (2019).

6. I. S. Cole, D. Lau, and D. A. Paterson, *Corrosion Engineering Science and Technology*, **39**, 209–218 (2004).

7. E. Schindelholz, R. G. Kelly, I. S. Cole, W. D. Ganther, and T. H. Muster, *Corrosion Science*, **67**, 233–241 (2013).

8. S. Li and L. H. Hihara, *J. Electrochem. Soc.*, **161**, C268–C275 (2014).

9. I. S. Cole, N. S. Azmat, A. Kanta, and M. Venkatraman, *International Materials Reviews*, **54**, 117–133 (2009).

10. I. Muto, E. Sato, and S. Ito, *Zairyo-to-Kankyo/Corrosion Engineering*, **42**, 714–720 (1993).

11. T. Shibata, H. Kurahashi, S. Kaneko, T. Ohya, and K. Motohashi, *Zairyo-to-Kankyo/Corrosion Engineering*, **44**, 281–286 (1995).

12. M. Nakata, N. Ono, and Y. Usuda, *Zairyo-to-Kankyo/Corrosion Engineering*, **46**, 559–564 (1997).

13. T. D. Weirich et al., *J. Electrochem. Soc.*, **166**, C3477–C3487 (2019).

14. R. M. Katona, J. C. Carpenter, A. W. Knight, C. R. Bryan, R. F. Schaller, R. G. Kelly, and E. J. Schindelholz, *Corrosion Science*, **177**, 108935 (2020).

15. J. Srinivasan and R. G. Kelly, *J. Electrochem. Soc.*, **163**, C768–C777 (2016).

16. R. E. Melchers, *Corrosion Science*, **47**, 2391–2410 (2005).

17. T. Mills, S. Prost-Domasky, K. Honeycutt, and C. Brooks, in *Corrosion Control in the Aerospace Industry*, S. Benavides, Editor, CRC Press LLC, Boca Raton, FL (2009).

18. Y. Kondo, *Corrosion*, **45**, 7–11 (1989).

19. I. Muto, E. Sato, S. Ito, and H. Kihira, in *Proceedings of the International Symposium on Plant Aging and Life Prediction of Corrodible Structures*, p. 153–160, NACE, Houston, TX (1997).

20. T. Shibata, *CORROSION*, **52**, 813–830 (1996).

21. Y. Tadokoro and A. Takahashi, *Zairyo-to-Kankyo*, **48**, 34–40 (1999).

22. P. J. Laycock, R. A. Cottis, and P. A. Scarf, *J. Electrochem. Soc.*, **137**, 64–69 (1990).

23. P. J. Laycock and P. A. Scarf, *Corrosion Science*, **35**, 135–145 (1993).

24. R. E. Melchers, *Probabilistic Engineering Mechanics*, **23**, 482–488 (2008).

25. R. F. Schaller, C. F. Jove-Colon, J. M. Taylor, and E. J. Schindelholz, *npj Materials Degradation*, **1**, 20 (2017).

26. R. E. Melchers, *npj Mater. Degrad.*, **3**, 1–7 (2019).

27. N. V. Smirnov, *Uspekhi Mathematicheskikh Nauk/Russian Mathematical Surveys*, **10**, 179–206 (1944).

28. G. E. Noether, in *Studies in Statistics*, Studies in Mathematics. R. V. Hogg, Editor, p. 39–65, Mathematical Association of America, Washington, DC (1978).

29. M. T. Woldemedhin, M. E. Shedd, and R. G. Kelly, *J. Electrochem. Soc.*, **161**, E3216–E3224 (2014).

30. K. Eguchi, T. L. Burnett, and D. L. Engelberg, *Corrosion Science*, **165**, 108406 (2020).

31. T. Shibata and T. Takeyama, *Corrosion*, **33**, 243–251 (1977).

32. K. Hebert and R. Alkire, *J. Electrochem. Soc.*, **135**, 2447–2452 (1988).

33. N. Sato, *J. Electrochem. Soc.*, **129**, 260–264 (1982).

34. Z. Y. Chen and R. G. Kelly, *J. Electrochem. Soc.*, **157**, C69–C78 (2010).

35. Z. Y. Chen, F. Cui, and R. G. Kelly, *J. Electrochem. Soc.*, **155**, C360–C368 (2008).

36. R. P. Gangloff, in *Environment-Induced Cracking of Materials*, S. A. Shipilov, R. H. Jones, J.-M. Olive, and R. B. Rebak, Editors, p. 141–165, Elsevier, Amsterdam (2008).

37. T. Kanezaki, C. Narazaki, Y. Mine, S. Matsuoka, and Y. Murakami, *International Journal of Hydrogen Energy*, **33**, 2604–2619 (2008).

38. Y. Mine, Z. Horita, and Y. Murakami, *Acta Materialia*, **57**, 2993–3002 (2009).

39. G. Tammann, *Lehrbuch der Metallographie*, Second., Leopold Voss, Leipzig, Germany, (1923).

40. R. E. Melchers, *Corrosion Science*, **45**, 923–940 (2003).

41. N. Murer and R. G. Buchheit, *Corrosion Science*, **69**, 139–148 (2013).

42. F. Cui, F. J. Presuel-Moreno, and R. G. Kelly, *Corrosion Science*, **47**, 2987–3005 (2005).

43. C. Liu, J. Srinivasan, and R. G. Kelly, *J. Electrochem. Soc.*, **164**, C845–C855 (2017).

44. T. Tsuru, K.-I. Tamiya, and A. Nishikata, *Electrochimica Acta*, **49**, 2709–2715 (2004).

45. N. Mi, M. Ghahari, T. Rayment, and A. J. Davenport, *Corrosion Science*, **53**, 3114–3121 (2011).

46. E. Schindelholz, B. E. Risteen, and R. G. Kelly, *J. Electrochem. Soc.*, **161**, C450–C459 (2014).

47. Coles, Stuart, *An Introduction to Statistical Modeling of Extreme Values*, Springer-Verlag London Limited, London, United Kingdom, (2001).

48. P. M. Aziz, *Corrosion*, **12**, 35–46 (1956).

49. M. Marozzi, *Journal of Nonparametric Statistics*, **21**, 629–647 (2009).

50. M. Marozzi, *Communications in Statistics - Simulation and Computation*, **42**, 1298–1317 (2013).

51. C. Bryan and E. Schindelholz, in *Paper C2018-10516, CORROSION 2018*, NACE International, Houston, TX (2018).

52. R. M. Katona, A. W. Knight, E. J. Schindelholz, C. R. Bryan, R. F. Schaller, and R.G Kelly, *Electrochimica Acta*, **370**, 137696 (2021).

Fe	Cr	Ni	C	Mn	P	S	Si	Mo	N	Cu
71.94	18.14	8.09	0.06	0.87	0.032	0.004	0.41	0.17	0.05	0.23

Table 1: Composition of 304 SS used in this study (all values in weight per cent). Nominal composition is reported as received from vendor. Material is identical to that used in Weirich *et al*.[13]

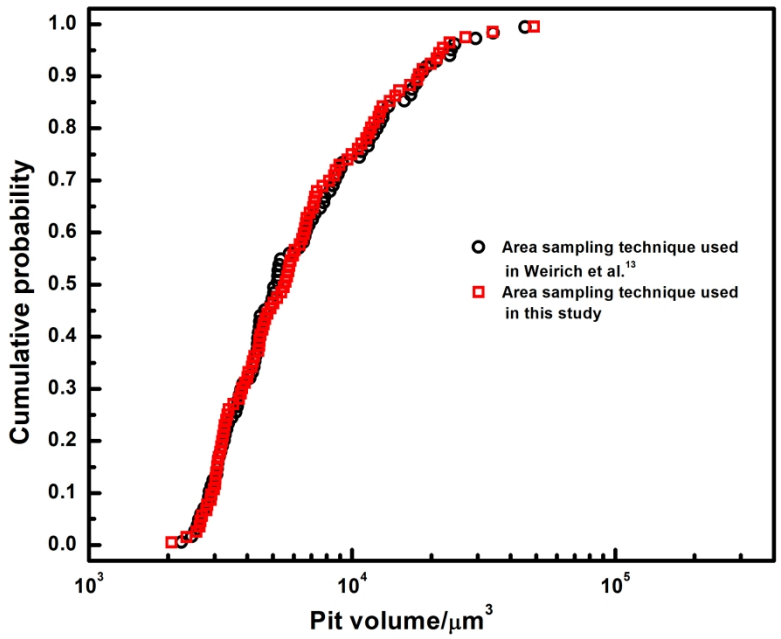

Figure 1. Comparison of the total pit volume distribution data obtained from profilometry using two different area sampling techniques on the same coupon (52 weeks, 76% RH). In order to aid visibility, data overlap among the different curves in (a) has been reduced by plotting every 2nd datapoint for the curves.

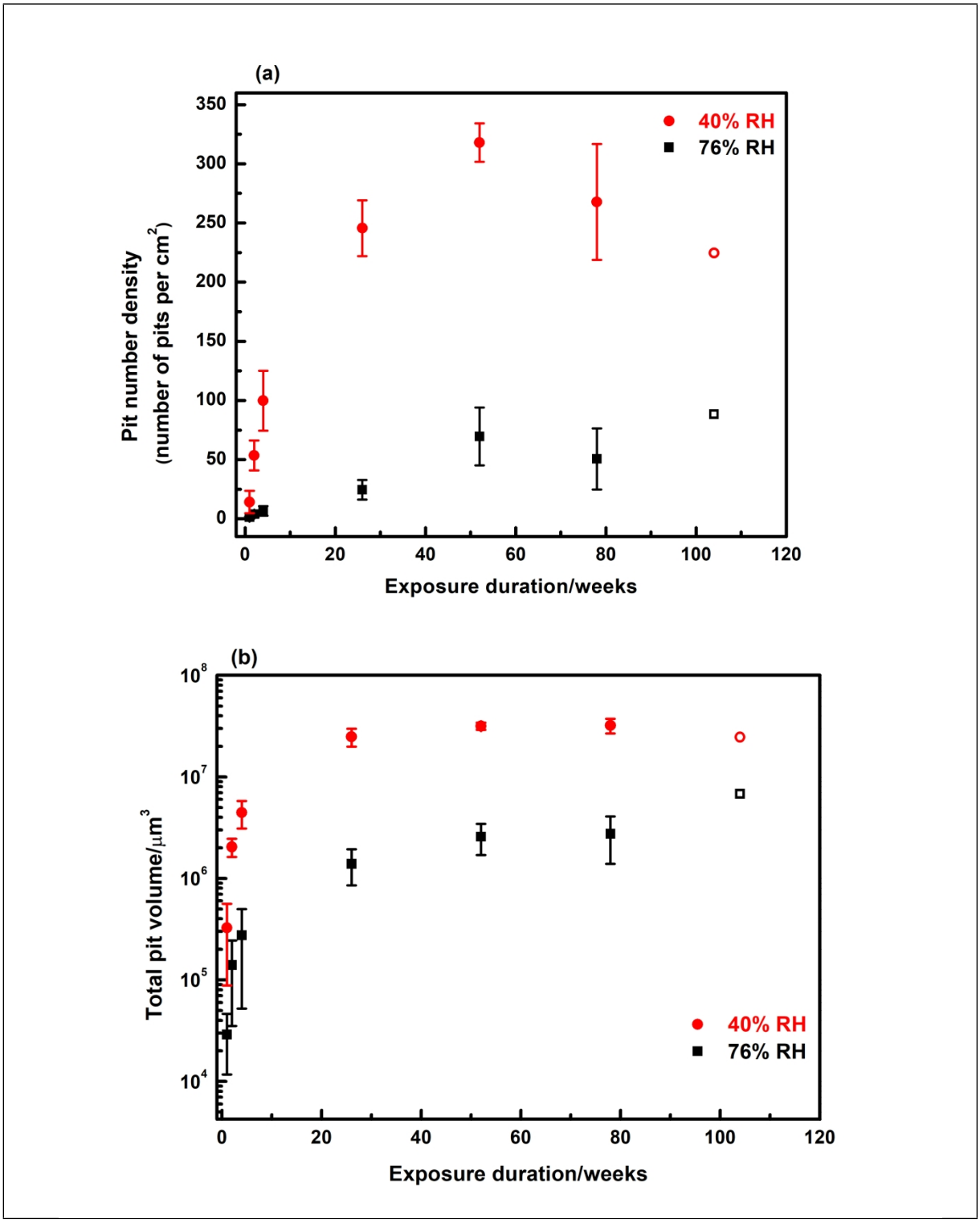
(a)
Pit number density
(number of pits per cm^2)
350
300
250
200
150
100
50
0
0
20
40
60
80
100
120
Exposure duration/weeks
40% RH
76% RH
(b)
Total pit volume/μm^3
10^8
10^7
10^6
10^5
10^4
0
20
40
60
80
100
120
Exposure duration/weeks
40% RH
76% RH

Figure 2. (a) Pit number density and (b) total pit volume as a function of exposure time for the 40% and 76% RH exposures. Error bars indicate standard deviation. Note that the datapoint corresponding to 104 weeks for either RH condition in each plot (open symbols) denotes the value of the single usable specimen at that timepoint. Datapoints corresponding to the other exposure durations denote the arithmetic mean (average) of the respective values measured in each of three replicate specimens.

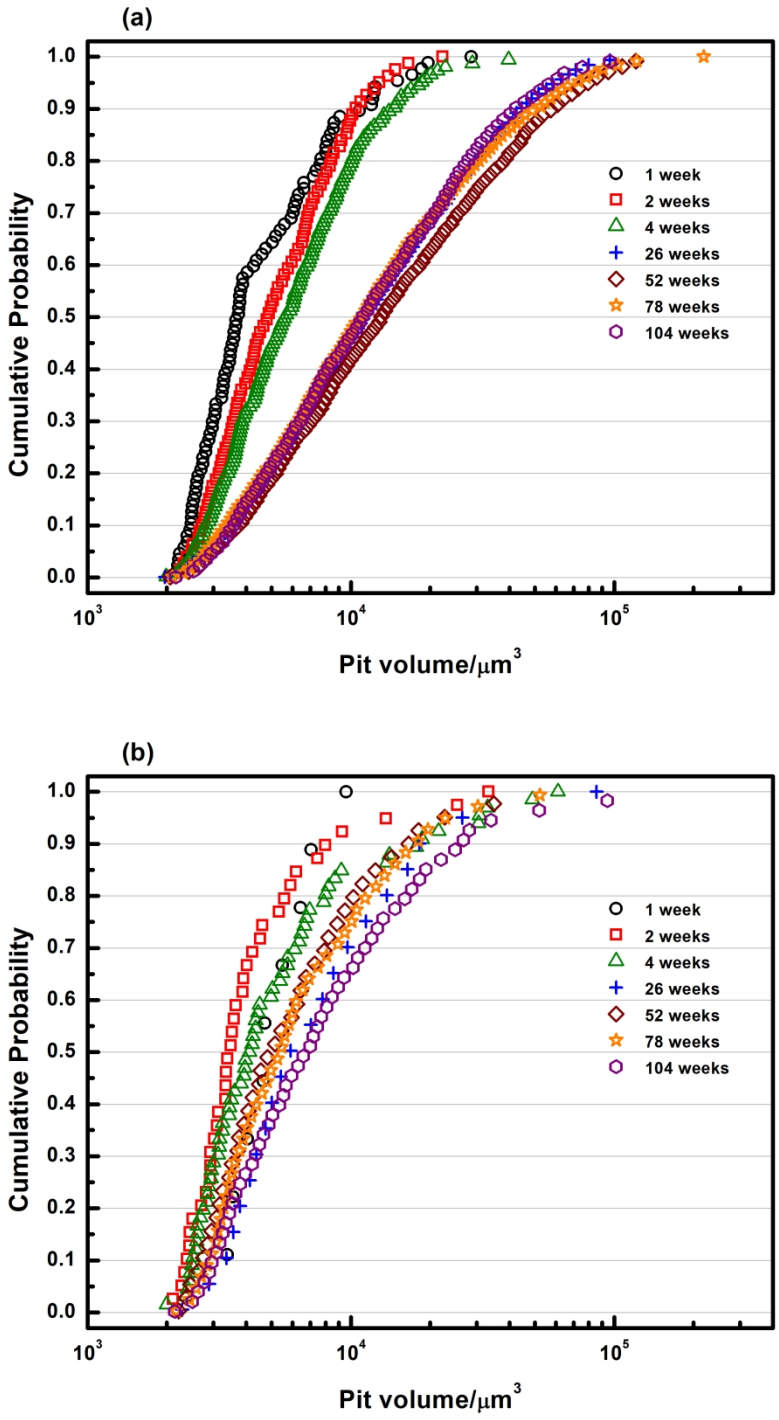
(a)
Cumulative Probability
Pit volume/μm3
1 week
2 weeks
4 weeks
26 weeks
52 weeks
78 weeks
104 weeks
(b)
Cumulative Probability
Pit volume/μm3
1 week
2 weeks
4 weeks
26 weeks
52 weeks
78 weeks
104 weeks

Figure 3. Time-evolution of corrosion damage plotted in terms of pit volume distribution at each timepoint for the (a) 40% RH and (b) 76% RH exposures.

In order to aid visibility, data overlap among the different curves in (a) has been reduced by plotting every 5th datapoint for the curves from the 2- and 4-week exposures, and every 15th datapoint for the curves from the 26-through 104-week exposures. Similarly in (b), every 5th datapoint for the curves from the 26-through 104-week exposures is plotted.

Further improvement in visibility is provided by differentiating the curves by color in the web version of this article.

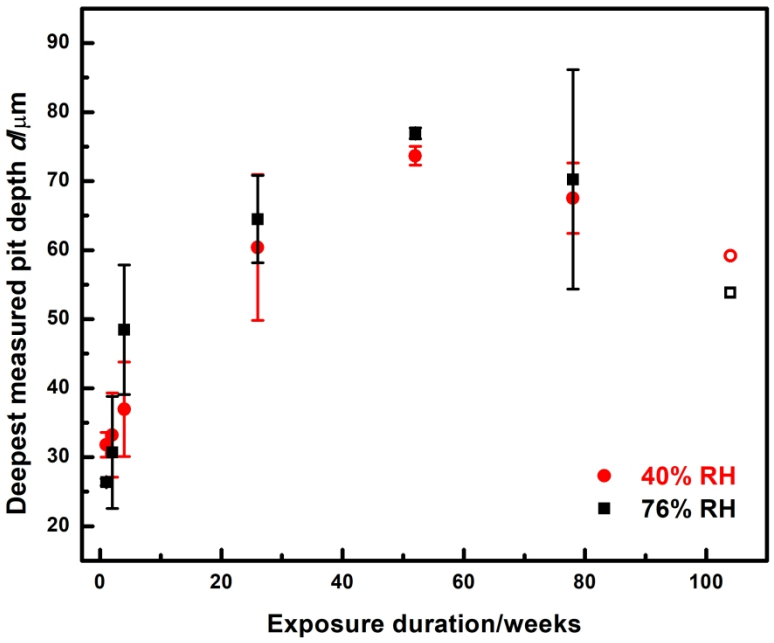

Figure 4. Depth of the deepest pit measured at each exposure time for the atmospheric exposures in the current study. Error bars indicate standard deviation. Note that the datapoint corresponding to 104 weeks for either RH condition in each plot (open symbols) denotes the value of the single usable specimen at that timepoint. Datapoints corresponding to the other exposure durations denote the arithmetic mean (average) of the depth of the deepest pit measured in each of three replicate specimens.

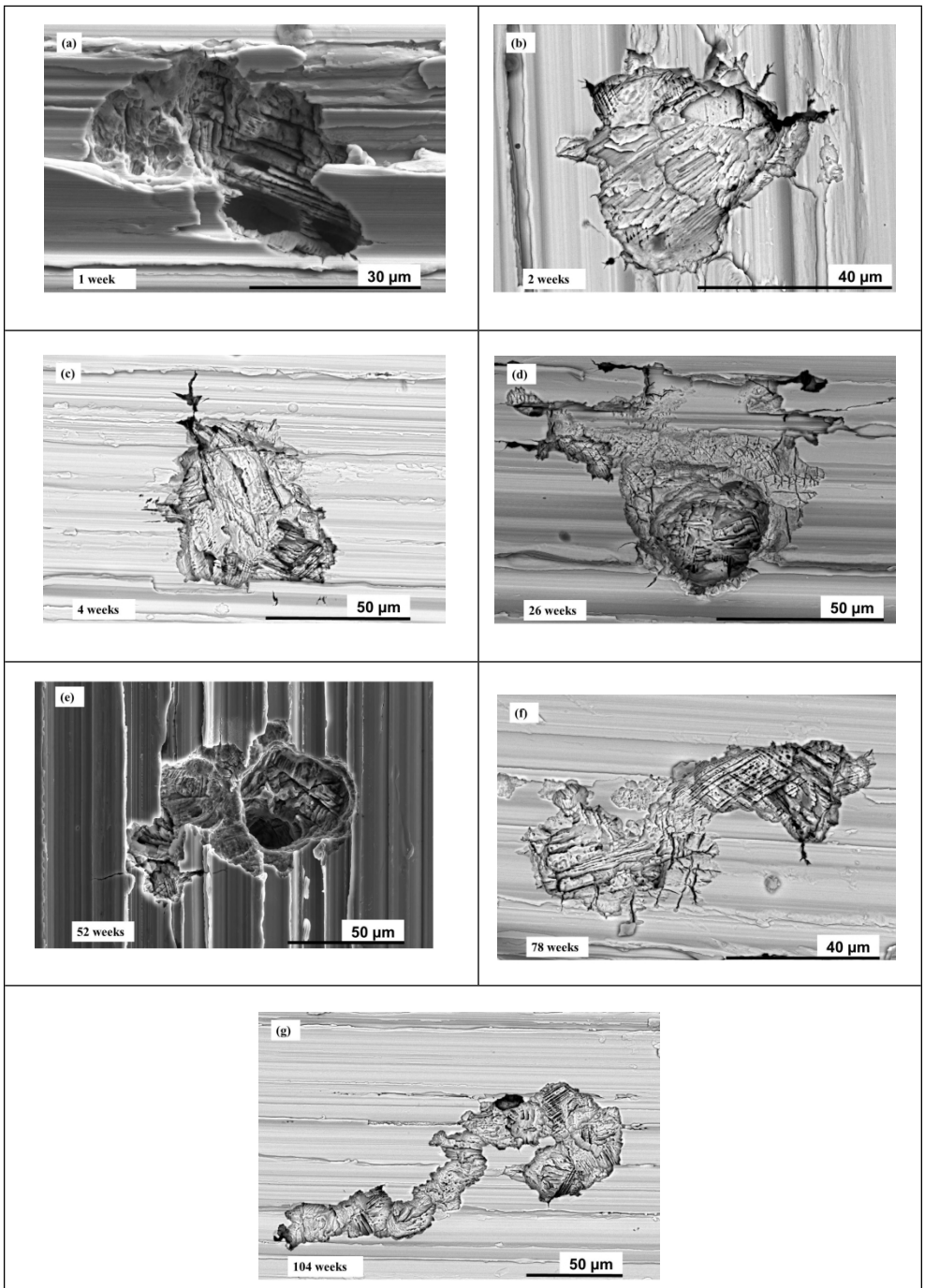

Figure 5. Secondary electron images from SEM indicating pit morphology differences following exposure for different times at 40% RH. Note the distinct irregular cross-hatching observed in the pits.

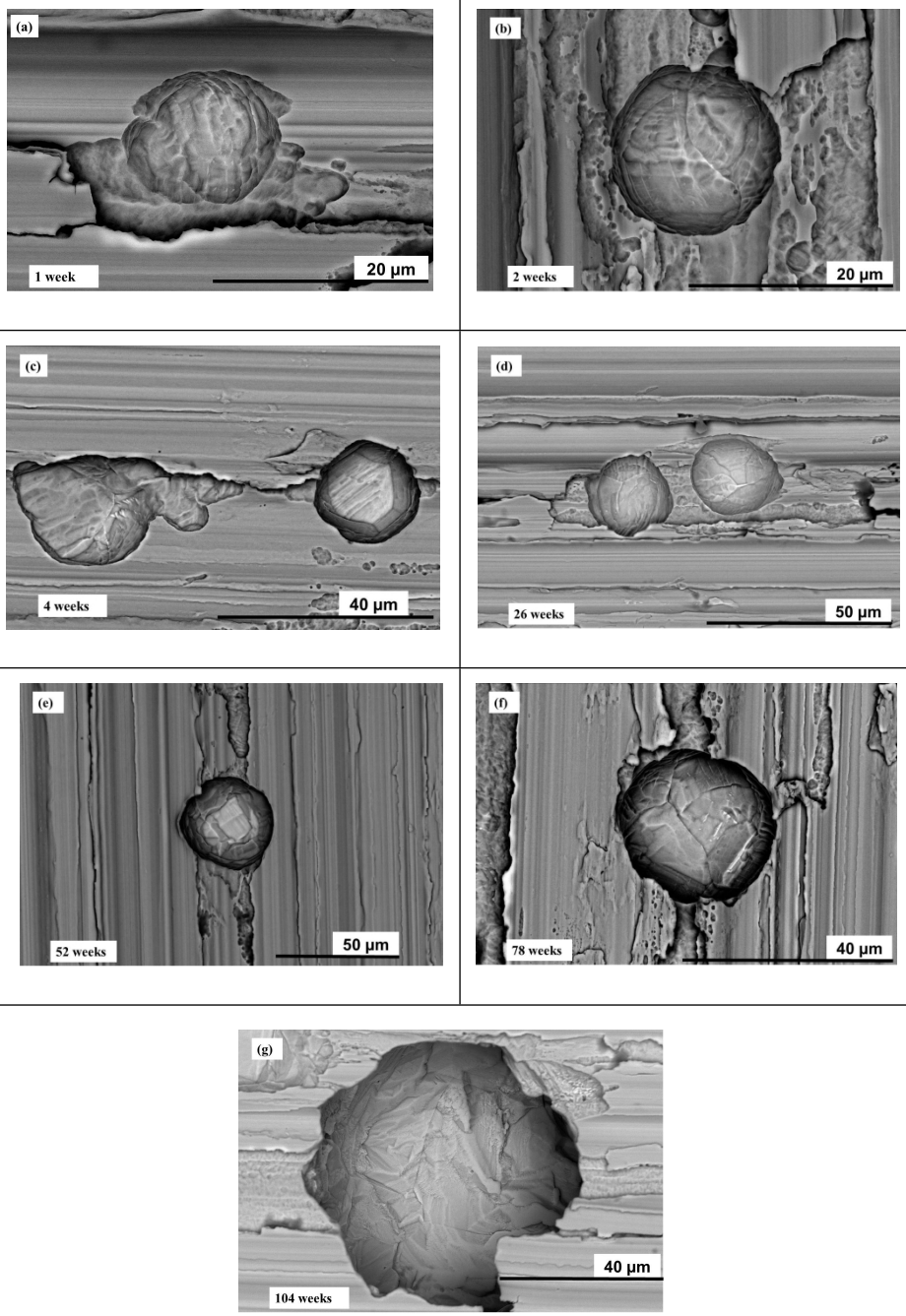

Figure 6. Secondary electron images from SEM indicating pit morphology differences following exposure for different times at 76% RH. Note the faceting observed in the pits.

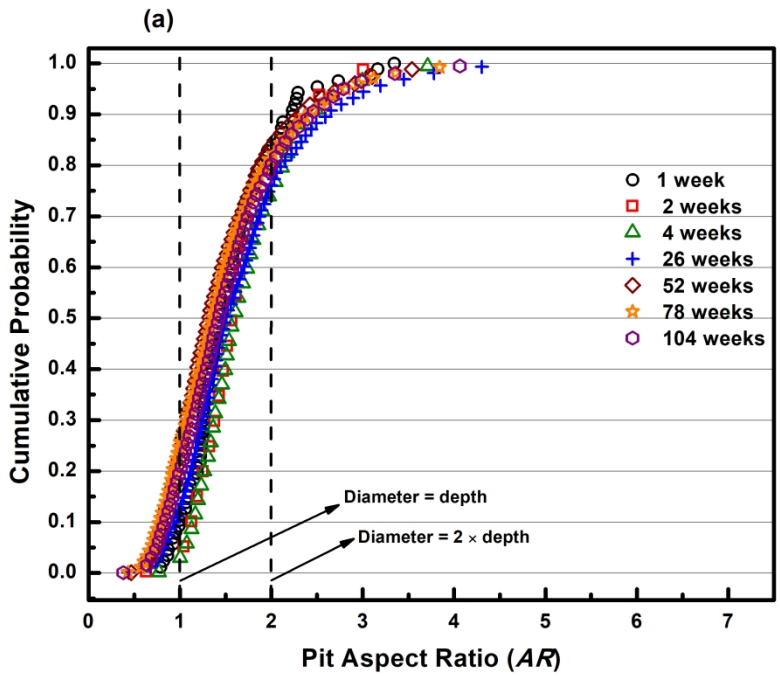
(a)
Cumulative Probability
Pit Aspect Ratio (AR)
1 week
2 weeks
4 weeks
26 weeks
52 weeks
78 weeks
104 weeks
Diameter = depth
Diameter = 2 × depth

Figure 7. Time-

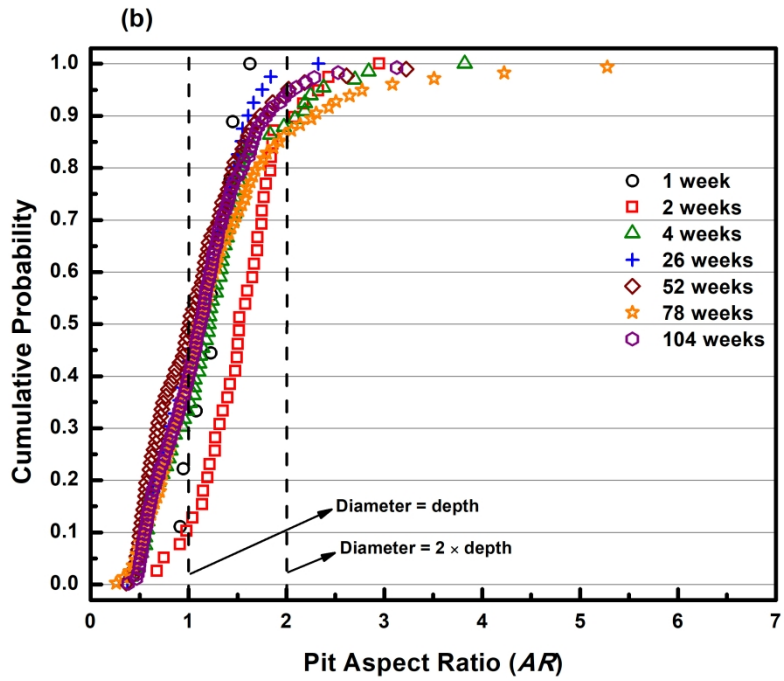

evolution of pit geometry plotted in terms of pit aspect ratio (*AR*) distribution at each timepoint for the (a) 40% RH and (b) 76% RH exposures. *AR* was calculated by dividing the measured pit diameter by the measured pit depth.

In order to aid visibility, data overlap among the curves in (a) has been reduced by plotting every 20th datapoint for the curves from the 2- through 104-week exposures.

Similarly in (b), every 5th datapoint for the curves from the 26-through 104-week exposures is plotted.

Further improvement in visibility is provided by differentiating the curves by color in the web version of this article.

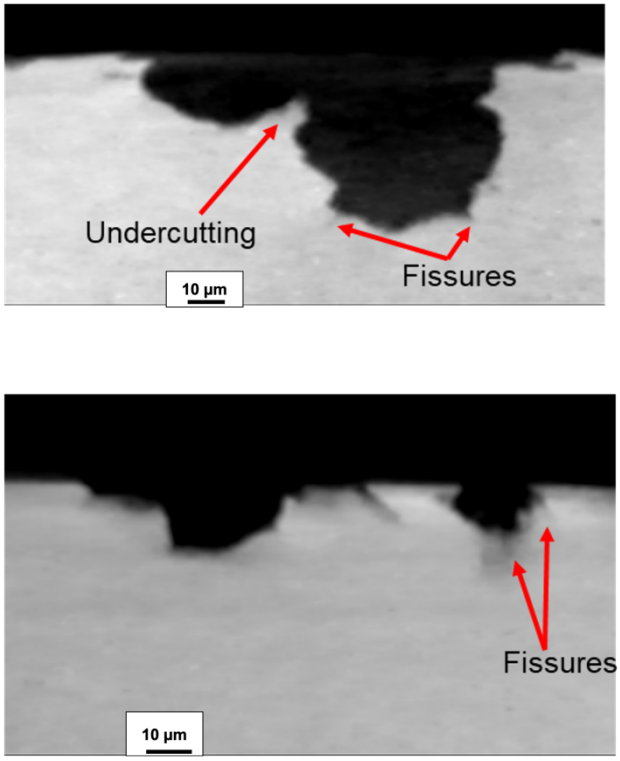

Figure 8. Cross-sectional slices of XCT scans. Possible fissures/microcracks emanating from the pit base and undercutting are indicated in the images. Images shown in the figure are at the maximum resolution of the technique.

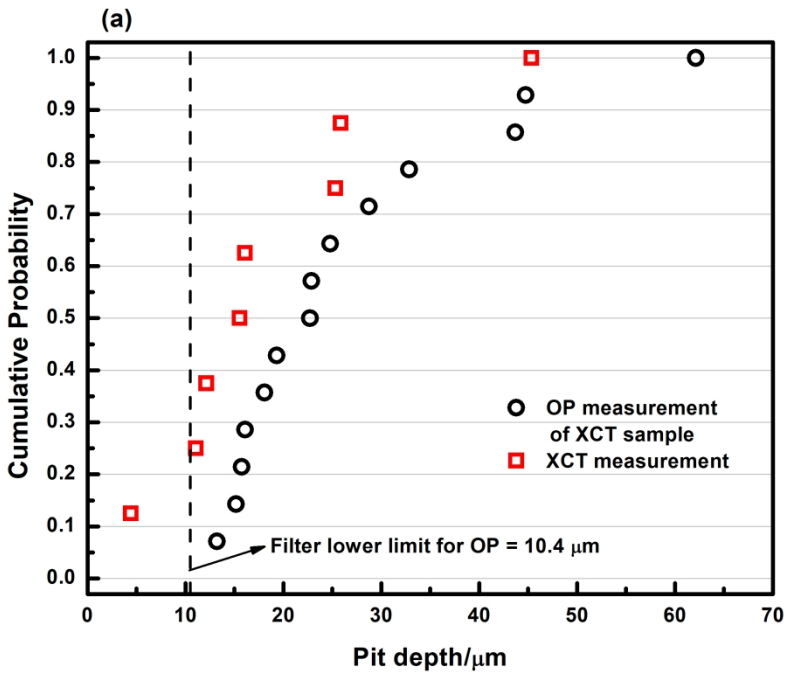
(a)
Cumulative Probability
Pit depth/μm
OP measurement
of XCT sample
XCT measurement
Filter lower limit for OP = 10.4 μm
0.0
0.1
0.2
0.3
0.4
0.5
0.6
0.7
0.8
0.9
1.0
0
10
20
30
40
50
60
70

Figure 9.

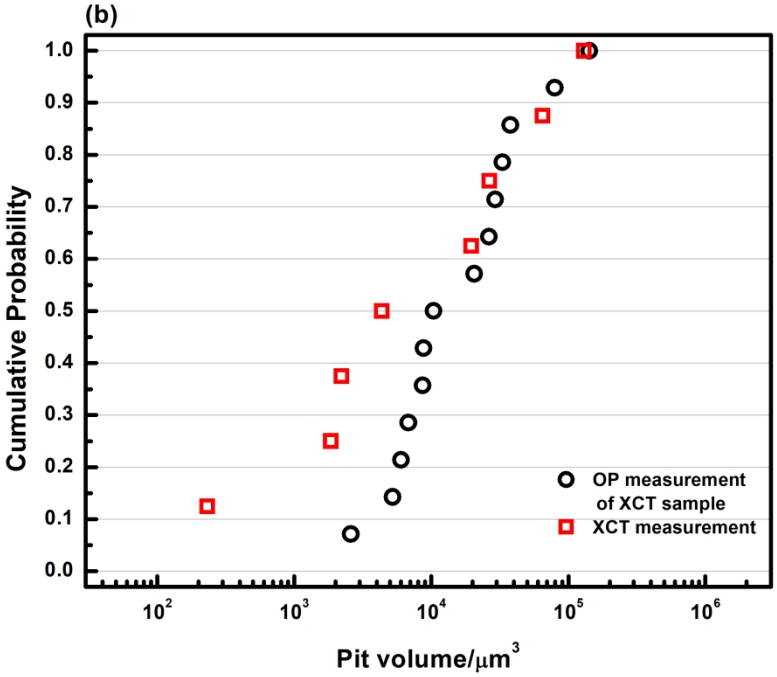

Comparison of geometric data collected by OP and XCT in terms of distributions of (a) pit depth and (b) pit volume.

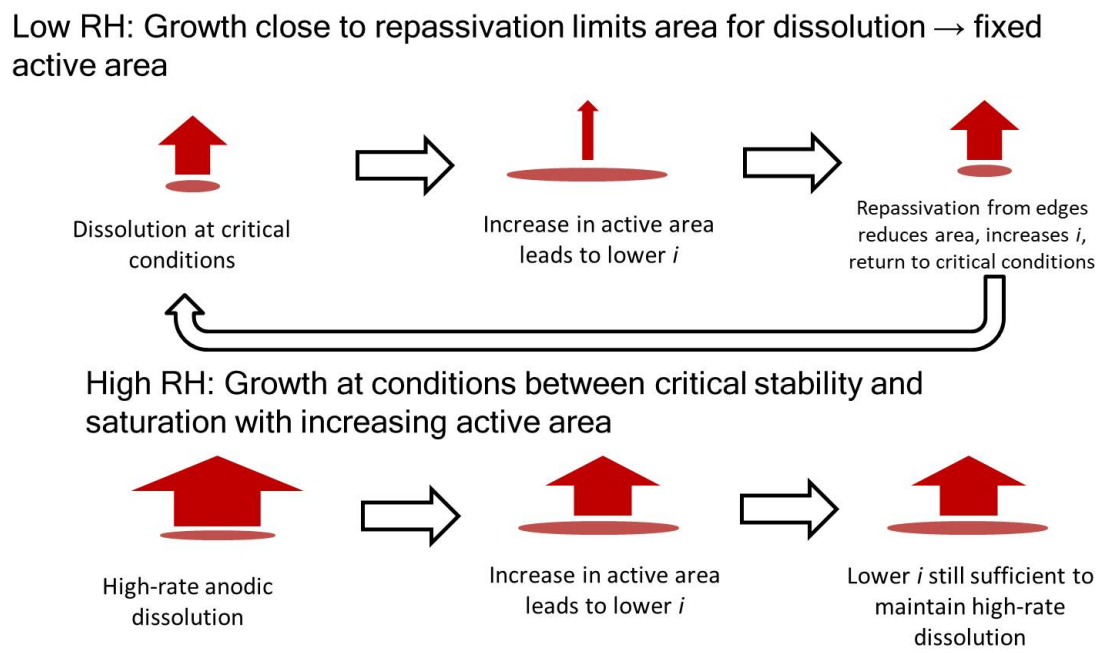

Figure 10. Schematic outline of the electrochemical rationale for observed difference in pit morphology between RH conditions.

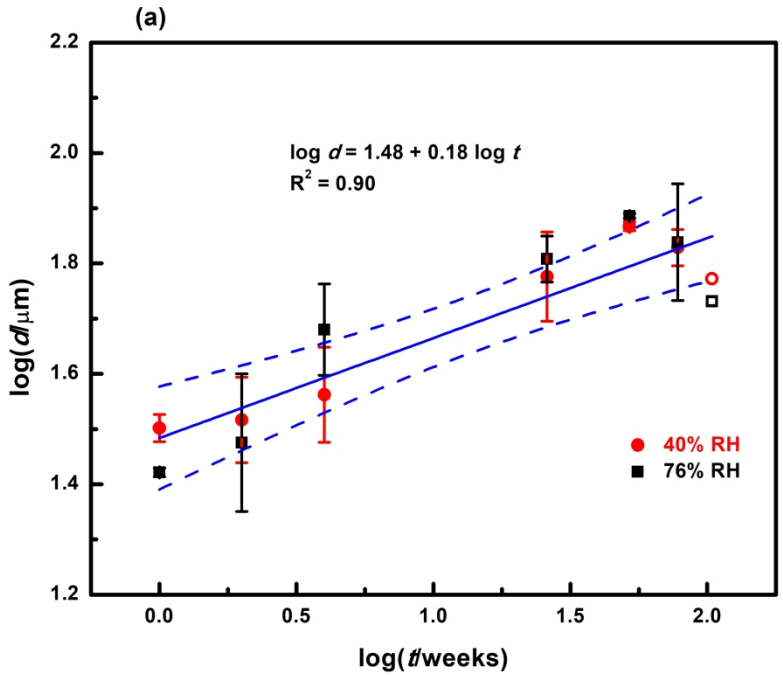
(a)
log d = 1.48 + 0.18 log t
R2 = 0.90
40% RH
76% RH
log(d/μm)
log(t/weeks)
2.2
2.0
1.8
1.6
1.4
1.2
0.0
0.5
1.0
1.5
2.0

Figure 11. Pitting

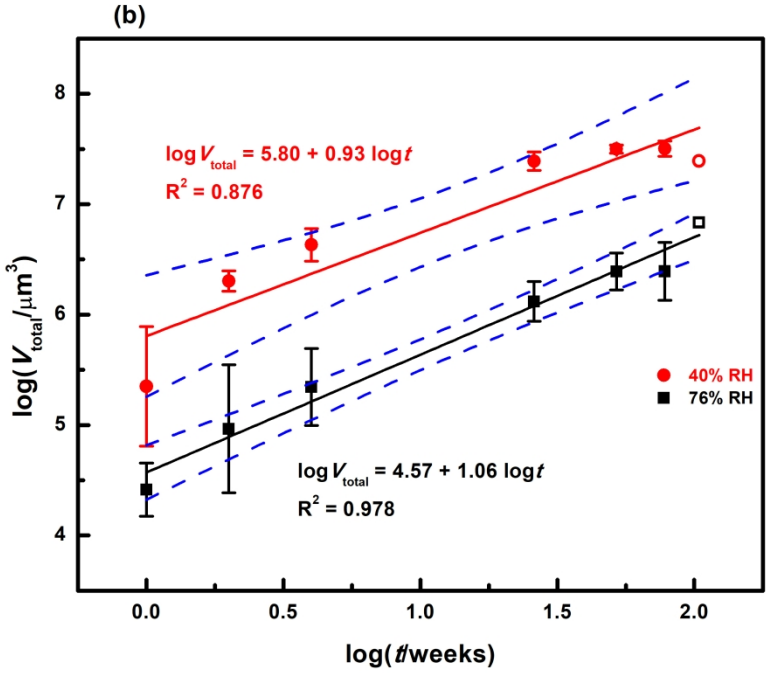

damage as a function of exposure duration, presented as log-log plots of (a) Depth of the deepest pit measured vs. exposure duration and (b) Total pit volume vs. exposure duration. Error bars indicate standard deviation. Note that the datapoint corresponding to 104 weeks for either RH condition in each plot (open symbols) denotes the value of the single usable specimen at that timepoint. Datapoints corresponding to the other exposure durations denote the arithmetic mean (average) of the respective values measured in each of three replicate specimens. The dashed blue lines contain the 95% confidence intervals corresponding to the respective fits.

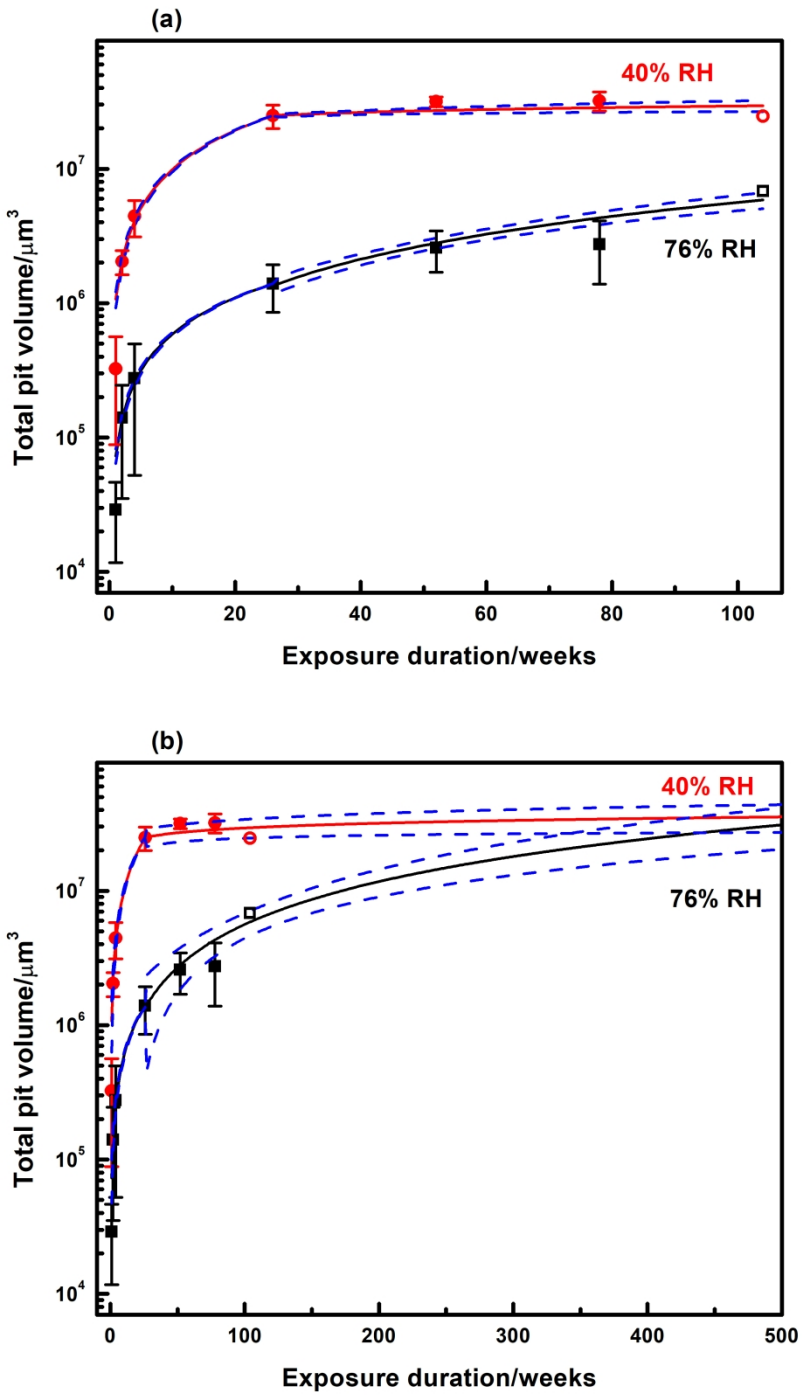
(a)
40% RH
76% RH
Total pit volume/μm3
Exposure duration/weeks
(b)
40% RH
76% RH
Total pit volume/μm3
Exposure duration/weeks

Figure 12. Corrosion damage modeled by piecewise fitting of the mean pit volume as a function of exposure duration. (a) Piecewise fitting function to the experimental exposure data with two power-law expressions, one fit to the exposure data up to 26 weeks, and another fit to the exposure data from 26 weeks to 104 weeks. Parameters corresponding to these fitting equations are listed in Table 2. The solid blue line is the fitting curve and the dashed blue lines contain the 95% confidence interval of the fit. (b) Corrosion damage prediction for a 10-year (500-week) period using the power-law parameters of the function fitting the exposure data from 26 weeks to 104 weeks. Error bars indicate standard deviation. Note that the datapoint corresponding to 104 weeks for either RH condition in each plot (open symbols) denotes the value of the single usable specimen at that timepoint. Datapoints corresponding to the other exposure durations denote the arithmetic mean (average) of the respective values measured in each of three replicate specimens.The dashed blue lines contain the 95% prediction interval corresponding to the fit.

$V_{total}(t) = a \cdot t^b$					
RH/%	**Exposure duration *t*/weeks**	**a/(× 10^6 μm^3)**	**95% confidence interval lower limit**	**b**	**95% confidence interval lower limit**
			95% confidence interval upper limit		**95% confidence interval upper limit**
40	[0, 26]	1.069	0.9538	0.9659	0.9328
			1.184		0.9989
	[26, 104]	17	13.62	0.1183	0.06015
			20.38		0.1765
76	[0, 26]	0.07311	0.06601	0.9045	0.8747
			0.08021		0.9343
	[26, 104]	0.04235	0.0239	1.061	0.947
			0.06161		1.175

Table 2: Power law expression parameters used in piecewise fitting in Figure 12 (a).